THE EUROPEAN
PHYSICAL JOURNAL C

Instability of Reissner–Nordström black hole in Einstein-Maxwell-scalar theory

Yun Soo Myung[1,a], **De-Cheng Zou**[1,2,b]

[1] Institute of Basic Sciences and Department of Computer Simulation, Inje University Gimhae, Gimhae 50834, Korea
[2] Center for Gravitation and Cosmology and College of Physical Science and Technology, Yangzhou University, Yangzhou 225009, China

Abstract The scalarization of Reissner–Nordström black holes was recently proposed in the Einstein-Maxwell-scalar theory. Here, we show that the appearance of the scalarized Reissner–Nordström black hole is closely related to the Gregory-Laflamme instability of the Reissner–Nordström black hole without scalar hair.

1 Introduction

Recently, the scalarized black hole solutions were found from Einstein-scalar-Gauss-Bonnet (ESGB) theories [1,2]. We note that these black holes with scalar hair are connected to the appearance of instability for the Schwarzschild black hole without scalar hair. Interestingly, the instability of Schwarzschild black hole in ESGB theory is regarded as not the tachyonic instability but the Gregory-Laflamme (GL) instability [3] by comparing it with the instability of the Schwarzschild black hole in the Einstein-Weyl gravity [4].

The notion of the GL instability comes from the three observations [5–8]: (1) the instability is based on the $s(l = 0)$-mode perturbations for scalar and tensor fields. (2) The linearized equation includes an effective mass term, providing that the potential develops negative region near the black hole horizon but it becomes positive after crossing the r-axis. (3) The instability of a black hole without hair is closely related to the appearance of a newly black hole with hair.

More recently, a scalarization of the Reissner–Nordström (RN) black hole was proposed in the Einstein-Maxwell-scalar (EMS) theory which is considered as a simpler theory than the ESGB theory [9]. We note that the scalarized black holes were found in the Einstein-scalar-Born-Infeld theory [10,11], regarded as a generalized EMS theory. The EMS theory includes three physically propagating modes of scalar, vector, and tensor. In this case, the instability of RN black hole is determined solely by the linearized scalar equation because the RN black hole is stable against tensor-vector perturbations, as found in the Einstein-Maxwell theory [12–15].

In this work, we wish to show that the appearance of the scalarized RN black hole is closely associated with the GL instability of the RN black hole without scalar hair. Here, the GL instability will be determined by solving the linearized scalar equation. This will indicate an important connection between scalarized RN black holes and GL instability of RN black holes.

The organization of our work is as follows. We introduce the EMS theory and its linearized theory around the RN black hole background in Sect. 2. In Sect. 3, we perform the stability analysis for the RN black hole based on the linearized scalar Eq. (18). Mainly, we derive the GL instability bound (20). We solve the static linearized Eq. (22) to confirm the threshold of the instability α_{th} as well as to obtain $n = 0, 1, 2 \cdots$ scalarized RN black holes in Sect. 4. In Sect. 5, we explore what the GL instability is. Section 6 is devoted to obtaining a scalarized RN black hole by solving the four Eqs. (41)–(44) numerically. It indicates that the appearance of the scalarized RN black hole is closely related to the GL instability of the RN black hole without scalar hair. Also, we obtain scalarized RN black holes for the quadratic coupling of $\alpha \phi^2$ for comparison to the exponential coupling $e^{\alpha \phi^2}$. Finally, we will describe our main results in Sect. 7.

2 EMS and its linearized theory

The EMS theory is given by [9]

$$S_{\text{EMS}} = \frac{1}{16\pi} \int d^4x \sqrt{-g} \Big[R - 2\partial_\mu \phi \partial^\mu \phi - V_\phi - e^{\alpha \phi^2} F^2 \Big],$$

$$\tag{1}$$

[a] e-mail: ysmyung@inje.ac.kr
[b] e-mail: dczou@yzu.edu.cn

where ϕ is the scalar field with a potential V_ϕ, α is a positive coupling constant, and $F^2 = F_{\mu\nu}F^{\mu\nu}$ is the Maxwell kinetic term. Here we choose $V_\phi = 0$ for simplicity. This theory implies that three of scalar, vector, and tensor are physically dynamical fields. It is noted that a different dilaton coupling of $e^{-2\alpha_0\phi}$ was introduced for the Einstein-Maxwell-dilaton theory originating from a low-energy limit of string theory [16,17]. Moreover, a quadratic coupling of $\alpha\phi^2$ will be considered as the other model to reveal scalarized charged black holes in Sect. 7.

Now, let us derive the Einstein equation from the action (1)

$$G_{\mu\nu} = 2\partial_\mu\phi\partial_\nu\phi - (\partial\phi)^2 g_{\mu\nu} + 2e^{\alpha\phi^2}T_{\mu\nu}, \qquad (2)$$

where $G_{\mu\nu} = R_{\mu\nu} - (R/2)g_{\mu\nu}$ is the Einstein tensor and $T_{\mu\nu} = F_{\mu\rho}F_\nu{}^\rho - F^2 g_{\mu\nu}/4$ is the Maxwell energy-momentum tensor. The Maxwell equation is given by

$$\nabla^\mu F_{\mu\nu} - 2\alpha\phi\nabla^\mu(\phi)F_{\mu\nu} = 0. \qquad (3)$$

The scalar equation takes the form

$$\Box\phi - \frac{\alpha}{2}e^{\alpha\phi^2}F^2\phi = 0. \qquad (4)$$

Considering $\bar{\phi} = 0$ and electrically charged $\bar{A}_t = Q/r$, one finds the RN solution from (2) and (3)

$$ds^2_{\rm RN} = \bar{g}_{\mu\nu}dx^\mu dx^\nu = -f(r)dt^2 + \frac{dr^2}{f(r)} + r^2 d\Omega_2^2 \qquad (5)$$

with the metric function

$$f(r) = 1 - \frac{2M}{r} + \frac{Q^2}{r^2}. \qquad (6)$$

Here, the outer horizon is located at $r = r_+ = M + \sqrt{M^2 - Q^2} = M(1 + \sqrt{1 - q^2})$ with $q = Q/M$, while the inner horizon is at $r = r_- = M(1 - \sqrt{1 - q^2})$. It is worth noting that (5) dictates a charged black hole solution without scalar hair. We stress that the RN solution (5) is a black hole solution to the EMS theory for any value of α. Hereafter we are interested in the outer horizon.

In order to explore the stability analysis, one has to obtain the linearized theory which describes the metric perturbation $h_{\mu\nu}$, vector perturbation a_μ and scalar perturbation φ propagating around the RN background (5) denoting by‾(overbar). By linearizing (2), (3), and (4), we find three linearized equations as

$$\delta G_{\mu\nu}(h) = 2\delta T_{\mu\nu}, \qquad (7)$$

$$\bar{\nabla}^\mu f_{\mu\nu} = 0, \qquad (8)$$

$$\left(\bar{\Box} + \alpha\frac{Q^2}{r^4}\right)\varphi = 0, \qquad (9)$$

where the linearized Einstein tensor $\delta G_{\mu\nu}$, the linearized energy-momentum tensor $\delta T_{\mu\nu}$, and the linearized Maxwell tensor $f_{\mu\nu}$ are given by

$$\delta G_{\mu\nu} = \delta R_{\mu\nu} - \frac{1}{2}\bar{g}_{\mu\nu}\delta R - \frac{1}{2}\bar{R}h_{\mu\nu}, \qquad (10)$$

$$\delta T_{\mu\nu} = \bar{F}_\nu{}^\rho f_{\mu\rho} + \bar{F}_\mu{}^\rho f_{\nu\rho} - \bar{F}_{\mu\rho}\bar{F}_{\nu\sigma}h^{\rho\sigma}$$
$$+\frac{1}{2}(\bar{F}_{\kappa\eta}f^{\kappa\eta} - \bar{F}_{\kappa\eta}\bar{F}^\kappa{}_\sigma h^{\eta\sigma})\bar{g}_{\mu\nu} - \frac{1}{4}\bar{F}^2 h_{\mu\nu}, \qquad (11)$$

$$f_{\mu\nu} = \partial_\mu a_\nu - \partial_\nu a_\mu. \qquad (12)$$

We note that an effective mass term of $-\alpha Q^2/r^4$ in (9) is replaced by $-2\lambda^2 M^2/r^6$ in the ESGB theory [4]. Here the scalar coupling constant '$\alpha > 0$' plays the role of a mass-like parameter.

3 Instability of RN black hole

In analyzing the stability of the RN black hole in the EMS theory, we first consider the two linearized Eqs. (7) and (8) because two perturbations of metric $h_{\mu\nu}$ and vector a_μ are coupled. Exactly, these correspond to the linearized equations for the Einstein-Maxwell theory. For the odd-parity perturbations, one found the Zerilli-Moncrief equation which describes two physical DOF propagating around the RN background [12,13]. Also, the even-parity perturbations with two physical degrees of freedom (DOF) were studies in [14,15]. It turns out that the RN black hole is stable against these perturbations. In this case, a massless spin-2 mode starts with $l = 2$, while a massless spin-1 mode begins with $l = 1$. The EMS theory provides $5(= 2 + 2 + 1)$ DOF propagating around the RN background.

Now, we focus on the linearized scalar Eq. (9) which determines the stability of the RN black hole in the EMS theory. Introducing

$$\varphi(t, r, \theta, \chi) = \frac{u(r)}{r}e^{-i\omega t}Y_{lm}(\theta, \chi), \qquad (13)$$

and considering a tortoise coordinate r_* defined by $dr_* = dr/f(r)$, a radial equation of (9) leads to the Schrödinger-type equation

$$\frac{d^2u}{dr_*^2} + \left[\omega^2 - V(r)\right]u(r) = 0, \qquad (14)$$

where the scalar potential $V(r)$ is given by

$$V(r) = f(r)\left[\frac{2M}{r^3} + \frac{l(l+1)}{r^2} - \frac{2Q^2}{r^4} - \alpha\frac{Q^2}{r^4}\right]. \qquad (15)$$

In Fig. 1, we find the α-dependent potentials for given $l = 0$, $M = 1.1$ and $q = M/Q = 0.418$ (a non-extremal RN black hole). The $s(l = 0)$-mode is allowed for the scalar

Fig. 1 The α-dependent potentials as function of $r \in [r_+, \infty)$ for the outer horizon radius $r_+ = 2.09(q = Q/M = 0.418)$ and $l = 0$. From the top, each curve represents the potential $V(r)$ of a scalar field for the parameter $\alpha = 19$ (stable), 19.83 (positive definite potential: sufficient condition for stability), 21, 25, 30.74 (sufficient condition for instability), and 35 (unstable case), respectively. The potentials have negative regions near the horizon for $\alpha > 19.83$. One conjectures that the threshold of GL instability occurs for $\alpha_{\text{th}} > 19.83$
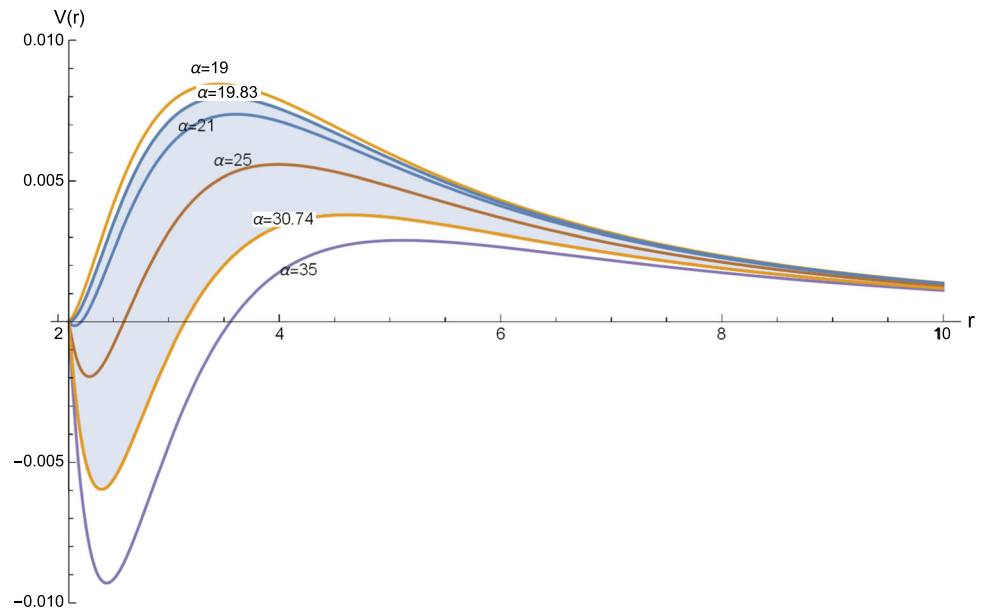
perturbation and it is regarded as an important mode to test the stability of the RN black hole. Hereafter, we consider this mode only.

A sufficient condition of $\int_{r_+}^{\infty} dr\, V(r)/f(r) < 0$ for instability [18,19] leads to the bound as

$$\alpha > \alpha_{\text{in}}(q) \equiv \frac{3}{q^2} - \frac{2q^2 - 3\sqrt{1-q^2}}{q^2}. \tag{16}$$

The first term $3/q^2$ was found in analyzing the black hole dynamics in Einstein-Maxwell-dilaton theory [16].

On the other hand, by observing the potential (15) carefully, the positive definite potential without negative region could be implemented by imposing the bound

$$\alpha \le \alpha_{\text{po}}(q) \equiv \frac{2(1-q^2)}{q^2} + \frac{2\sqrt{1-q^2}}{q^2}, \tag{17}$$

which guarantees a stable RN black hole. This is called the sufficient condition for stability. We note that (16) is not a necessary and sufficient condition for the instability. Observing Fig. 1 together with $q = 0.418$, one finds that two potentials with $\alpha = 21, 25$ between $\alpha_{\text{po}} = 19.83$ and $\alpha_{\text{in}} = 30.74$ develop negative regions near the horizon, but they become positive after crossing the r-axis.

At this stage, we would like to mention that such potentials exist around neutral black holes (black holes without charge) in higher dimensions and the S-deformation has been used to confirm the stability of neutral black holes in higher dimensions [20]. We conjecture that the GL instability may occur for $\alpha_{\text{th}} > 19.83$, but the threshold of instability α_{th} should be determined explicitly by the numerical computations. We expect that α_{th} is located at the shaded region between α_{in}

and α_{po}. Usually, if the potential V derived from physically propagating modes is negative in some region, a growing perturbation can appear in the spectrum. This might indicate an instability of the black hole system under such perturbations. However, this is not always true. Some potentials with negative region near the horizon do not imply the instability. The criterion to determine whether a black hole is stable or not against the perturbation is whether the time-evolution of the perturbation is decaying or not. The perturbed equation around a RN black hole can usually be described by the Schrödinger-type equation (18), where a growing mode like $e^{\Omega t}$ of the perturbation indicates the instability of the black hole. The absence of any unstable physical fields provides a precise way of determining the stability of the black hole.

It suggests that the RN black hole would be unstable for $\alpha > \alpha_{\text{th}} = 29.47$ with $q = 0.418$, while it is stable for $19.83 < \alpha < 29.47$ showing negative region near the horizon. In the latter case, the S-deformation method could provide a complementary result to support the stability of such black holes by finding the deformed potential [21,22].

To determine the threshold of instability explicitly, one has to solve the second-order differential equation numerically

$$\frac{d^2u}{dr_*^2} - \left[\Omega^2 + V(r)\right]u(r) = 0, \tag{18}$$

which allows an exponentially growing mode of $e^{\Omega t}$ ($\omega = i\Omega$) as an unstable mode. Here we choose two boundary conditions: a normalizable solution of $u(\infty) \sim e^{-\Omega r_*}$ at infinity and a solution of $u(r_+) \sim (r - r_+)^{\Omega r_+}$ near the outer horizon. Observing Fig. 2, we read off the threshold of instability $\alpha_{\text{th}}(q) = \{88.98, 60.69, 29.47, 15.46, 8.019, 2.995\}$ at $q = \{0.25, 0.3, 0.418, 0.55, 0.7, 0.9\} \equiv \{\cdots\}$. From

Fig. 2 Plots of unstable scalar modes (●) on six different curves with $q = \{0.25, 0.3, 0.418, 0.55, 0.7, 0.9\}$. The $y(x)$-axis denote Ω in $e^{\Omega t}$ (mass-like parameter α). Here we observe that the thresholds ($\Omega = 0$) of instability are located at $\alpha_{th}(q) \approx \{88.98, 60.69, 29.47, 15.46, 8.019, 2.995\}$
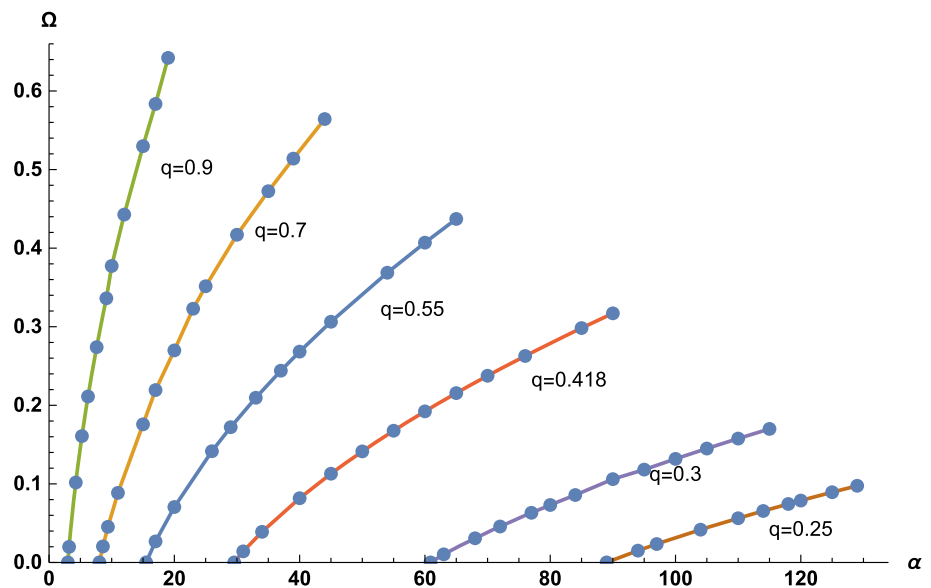

Fig. 3 Three α-curves as function of q. The upper blue curve represents $\alpha_{in}(q)$ in (16) and the middle green curve indicates $\alpha_{th}(q)$, while the lower red one denotes $\alpha_{po}(q)$ (17). We find an inequality of $\alpha_{po}(q) < \alpha_{th}(q) < \alpha_{in}(q)$
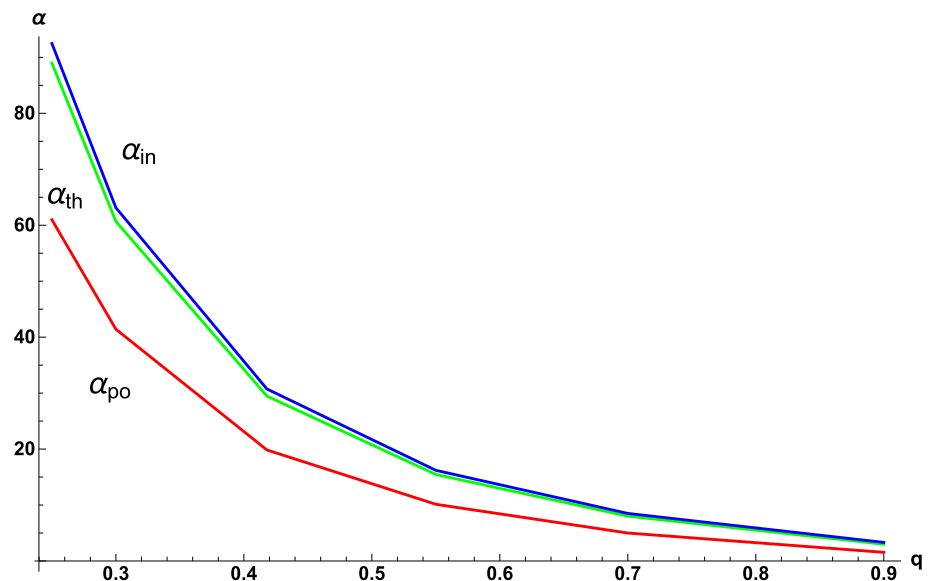

Fig. 3, one confirms that the threshold of instability is located between the sufficient condition for instability $\alpha_{in}(q) \approx \{92.48, 63.13, 30.74, 16.2, 8.45, 3.318\}$ at $q = \{\cdots\}$ and the sufficient condition for stability $\alpha_{po}(q) \approx \{68.98, 41.42, 19.83, 10.13, 4.997, 1.545\}$ at $q = \{\cdots\}$. This implies an inequality as

$$\alpha_{po}(q) < \alpha_{th}(q) < \alpha_{in}(q), \tag{19}$$

where $\alpha_{po}(q)$ and $\alpha_{in}(q)$ are given by (17) and (16), while $\alpha_{th}(q)$ is determined by solving (18) numerically.

Consequently, the GL instability bound for the RN black hole is given by

$$\alpha > \alpha_{th}(q) \tag{20}$$

which is considered as one of our main results. However, we could not determine an explicit form of $\alpha_{th}(q)$ as function of q like as $\alpha_{in}(q)$ in (16). In addition, the small unstable black appears when the bound satisfies

$$r_+ < r_c(q = 0.7) = 1.714 \tag{21}$$

at $\alpha = 8.019$.

4 Static scalar perturbation

Here, it is worth checking the instability bound (20) again because the precise value of $\alpha_{th}(q)$ determines scalarized RN black holes. This can be achieved by obtaining the static perturbed solutions to the linearized Eq. (14) with $\omega = 0$ on
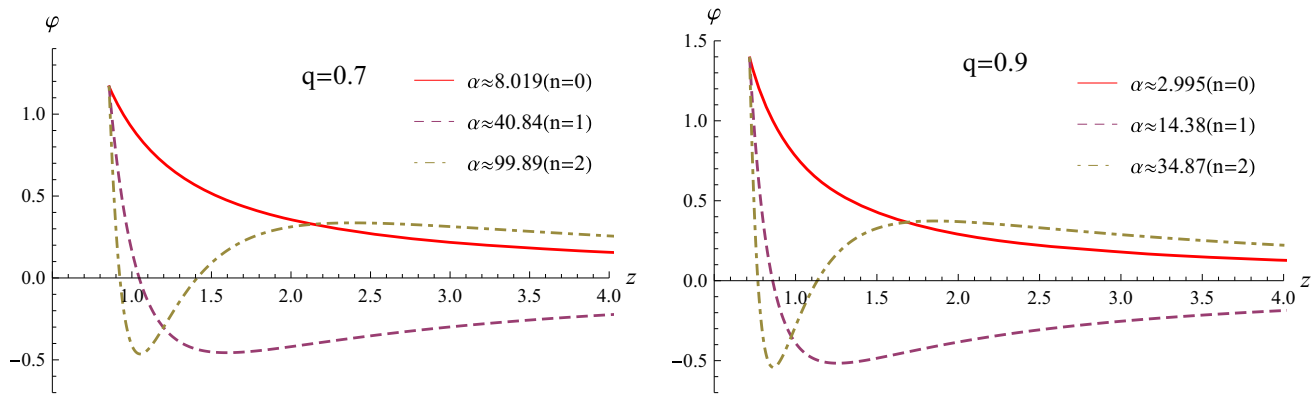
Fig. 4 Radial profiles of $\varphi = u(z)/z$ as function of $z = r/(2M)$ for the first three perturbed scalar solutions. The left-handed picture is depicted for $q = 0.7$, while the right-handed one is designed for the RN background. For a given $l = 0$ and q, requiring an asymptotically vanishing condition ($\varphi_\infty \to 0$) leads to the fact that the existence of a smooth scalar determines a discrete set for α. In addition, it determines $n = 0, 1, 2, \cdots$ branches of scalarized black holes. Introducing a static condition ($\omega = 0$) and a new coordinate of $z = r/2M$, the equation for $u(r)$ reduces to

$$f(z)u''(z) + f'(z)u'(z) - \left(\frac{\alpha q^2}{4z^4} - \frac{f'(z)}{z}\right)u(z) = 0, \quad (22)$$

where $f(z) = (z - z_-)(z - z_+)/z^2$ with $z_\pm = (1 \pm \sqrt{1 - q^2})/2$.

Here we wish to find a numerical solution even though an analytic solution is available for $l = 0$ case [9]. For this purpose, we first propose the near-horizon expansion for $u(z)$ as

$$u(z) = u_+ + u'_+(z - z_+) + \frac{u''_+}{2}(z - z_+)^2 + \cdots. \quad (23)$$

This expression can be used to set data outside the outer horizon for a numerical integration from $z = z_+$ to $z = \infty$. Here the coefficients u'_+ and u''_+ could be determined in terms of a free parameter u_+ as

$$u'_+ = -\frac{\alpha q^2 + 4z_+(z_- - z_+)}{4z_+^2(z_+ - z_-)}u_+,$$

$$u''_+ = \frac{\alpha q^2 \left(\alpha q^2 + 8z_-z_+\right)}{32z_+^4(z_+ - z_-)^2}u_+. \quad (24)$$

An asymptotic form of $u(z)$ near the infinity of $z = \infty$ is given by

$$u(z) = u_\infty + \frac{u^{(1)}}{z} + \frac{u^{(2)}}{z^2} + \cdots, \quad (25)$$

where two relations are expressed in terms of u_∞ as

$q = 0.9$ (near-extremal black hole). The number of nodes n is number of zero crossings. All profiles approach zero as $z \to \infty$

$$u^{(1)} = \frac{z_- + z_+}{2}u_\infty,$$

$$u^{(2)} = \frac{-\alpha q^2 + 8(z_-^2 + z_-z_+ + z_+^2)}{24}u_\infty. \quad (26)$$

At this stage, it is worth noting that we search for bound state scalar solution to (22) in the RN spacetime. We are free to choose the value of scalar field u_+ at the horizon because (22) is a linear differential equation and then, we choose $u_\infty = 1$ at infinity [2]. Actually, a numerical solution could be obtained by connecting the near-horizon form (23) to the asymptotic form (25) together with selecting the parameter α for given q properly. In this case, we obtain two discrete spectra of the parameter α: $\alpha_n(q = 0.7) \approx \{\underline{8.019}, 40.84, 99.89, \cdots\}$ and $\alpha_n(q = 0.9) \approx \{\underline{2.995}, 14.38, 34.87, \cdots\}$. The other four spectra are given by $\alpha_n(0.55) \approx \{\underline{15.46}, 80.02, 196.1, \cdots\}$, $\alpha_n(0.418) \approx \{\underline{29.47}, 153.9, 377.7, \cdots\}$, $\alpha_n(0.3) \approx \{\underline{60.69}, 318.4, 382.0, \cdots\}$, and $\alpha_n(0.25) \approx \{\underline{88.98}, 467.4, 1148, \cdots\}$. In Fig. 4, these solutions are classified by the order number $n = 0, 1, 2, \cdots$ which is identified with the number of nodes for $\varphi(z) = u(z)/z$. We find that the $n = 0$ scalar mode without zero crossing represents the fundamental branch of scalarized black holes, while the $n = 1, 2$ scalar modes with zero crossings denote $n = 1, 2$ higher branches of scalarized black holes. Actually, this corresponds to finding the $l = 0$ bifurcation points from the RN black hole with $q = Q/M$. Finally, we confirm that for given q, $\alpha_{n=0}(q) = \alpha_{\min}(q)$ [underline value] recovers the threshold of instability $\alpha_{th}(q)$ exactly.

5 GL instability

The instability of the RN black hole may be regarded as the GL instability since this instability is based on the

$s(l=0)$ mode of a perturbed scalar and its linearized equation includes an effective mass term (not tachyonic mass of $m_t^2 < 0$ presicely) which develops negative potential near the horizon from the Maxwell kinetic term. In this section, we wish to clarify the similarity and difference between the GL instability (modal instability) and tachyonic instability because the instability of RN black hole is closely related to appearance of scalarized RN black holes.

Let us first introduce the tachyon propagation with mass squared $m_t^2 < 0$ in the RN background as

$$\left(\bar{\Box} - m_t^2\right)\varphi_t = 0 \tag{27}$$

which provides a Schrödinger equation for radial part

$$\frac{d^2 u_t}{dr_*^2} + \left[\omega^2 - V_t(r)\right]u_t(r) = 0 \tag{28}$$

with the tachyon potential $V_t(r)$

$$V_t(r) = f(r)\left[\frac{2M}{r^3} + \frac{l(l+1)}{r^2} - \frac{2Q^2}{r^4} + m_t^2\right]. \tag{29}$$

As is shown Fig. 5, the potential $V_t(r)$ for $l = 0$ tachyonic mode develops a positive region near horizon, while it approaches -0.01 as $r \to \infty$ for $m_t^2 = -0.01$. This shows clearly the tachyonic instability of RN black hole because the sufficient condition for instability ($\int_{r_+}^{\infty} dr\, V_t(r)/f(r) = -\infty < 0$) is always satisfied with any mass $m_t^2 = -\text{const} < 0$. We wish to mention that V_t differs from $V(r)$ in (15) in the sense that the latter is negative near horizon and becomes positive after crossing the r-axis. We regard '$-\alpha Q^2/r^4$' in $V(r)$ as an effective mass term which can be made sufficiently negative by choosing α, making the scalar potential sufficiently negative in the near horizon. However, its role is limited to small r, because it approaches zero as $r \to \infty$. Such a r-dependent mass term is necessary to have the scalarized RN black holes.

Now we consider the stability of Schwarzschild black hole in Einstein-Weyl gravity whose action takes the form [6,8]

$$S_{EW} = \gamma \int d^4 x \sqrt{-g}\left[R - \frac{1}{2m_2^2}C_{\mu\nu\rho\sigma}C^{\mu\nu\rho\sigma}\right]. \tag{30}$$

Its linearized equation around the Schwarzschild black hole is given by the Licherowicz-Ricci tensor equation

$$(\Delta_L + m_2^2)\delta R_{\mu\nu} = 0, \tag{31}$$

where the Lichnerowicz operator is given by

$$\Delta_L \delta R_{\mu\nu} = -\bar{\Box}\delta R_{\mu\nu} - 2\bar{R}_{\mu\rho\nu\sigma}\delta R^{\rho\sigma}. \tag{32}$$
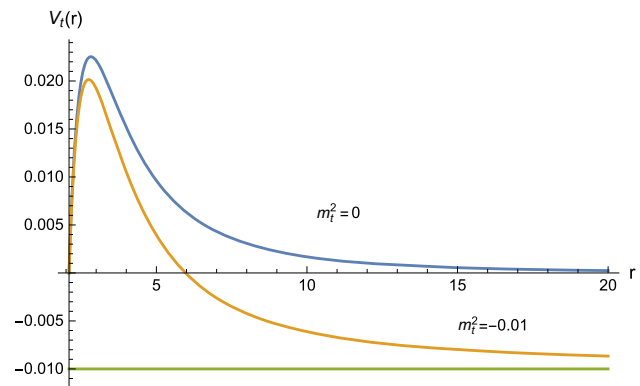
Fig. 5 The tachyonic potential $V_t(r)$ as function of $r \in [r_+, \infty)$ for the outer horizon radius $r_+ = 2.09(q = Q/M = 0.418)$ and $l = 0$. For comparison, we include a massless scalar potential with $m_t^2 = 0$

We note here that the condition of non-tachyonic mass requires $m_2^2 > 0$ because the Lichnerowicz operator contains $-\bar{\Box}$. Before we proceed, we would like to mention the GL instability. For this purpose, we consider the perturbations around the 5D black string with $ds_5^2 = ds_4^2 + dz^2$ where ds_4^2 denotes the Schwarzschild line element,

$$h_{MN}(t, r, \theta, \chi, z) = \begin{bmatrix} h_{\mu\nu}^{(4)} & h_{\mu z} \\ h_{z\nu} & h_{zz} \end{bmatrix},$$

where the z-dependence is assumed to be of the form e^{ikz} and the time-dependence takes the form of $e^{\Omega t}$. Actually, Eq. (31) takes the same form as the linearized black string equation for $h_{\mu\nu}^{(4)}$ with the transverse-traceless gauge [3]

$$(\Delta_L + k^2)h_{\mu\nu}^{(4)} = 0 \tag{33}$$

except that the mass m_2 of the Ricci tensor is replaced by the wave number k along z direction. The GL instability states that the 5D black string is unstable against the metric perturbation for $k < k_{th} = 0.876/r_+$ (long wavelength perturbation). The GL instability is an $s(l = 0)$-wave spherically symmetric instability from the four-dimensional perspective. In addition, it is interesting to note that the dRGT massive gravity having a Schwarzschild solution when formulated in a diagonal bimetric form, has the same linearized equation as (31) except replacing $\delta R_{\mu\nu}$ by $h_{\mu\nu}$ [23,24].

The $l = 0$ polar sector of Eq. (31) is given by

$$\frac{d^2\tilde{\varphi}_0}{dr_*^2} - \left[\Omega^2 + V_Z(r)\right]\tilde{\varphi}_0(r) = 0 \tag{34}$$

with $\tilde{\varphi}_0 = s(l = 0)$-mode of $\delta R_{\mu\nu}$ and the Zerilli potential $V_Z(r)$ [7,24]

$$V_Z(r) = \left(1 - \frac{r_+}{r}\right)$$
$$\times \left[\frac{r_+}{r^3} + m_2^2 - \frac{12r_+(r - 0.5r_+)m_2^2 + 6r^3(2r_+ - r)m_2^4}{(r_+ + r^3 m_2^2)^2}\right]. \tag{35}$$
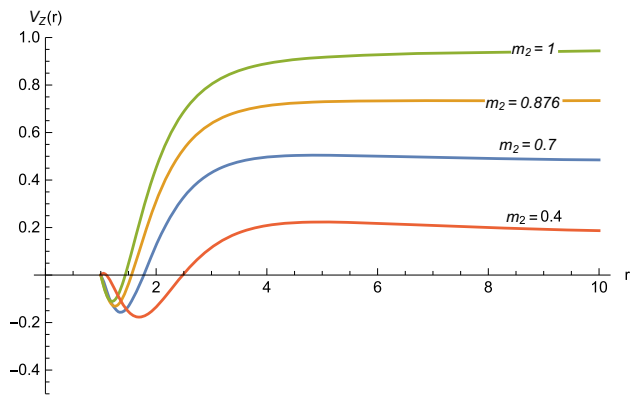
Fig. 6 The Zerilli potentials $V_Z(r)$ as function of $r \in [r_+, \infty)$ with different masses $m_2 = 1$ (stable), 0.876 (threshold), 0.7 (unstable), 0.4(unstable) for the horizon radius $r_+ = 2M = 1$ and $l = 0$
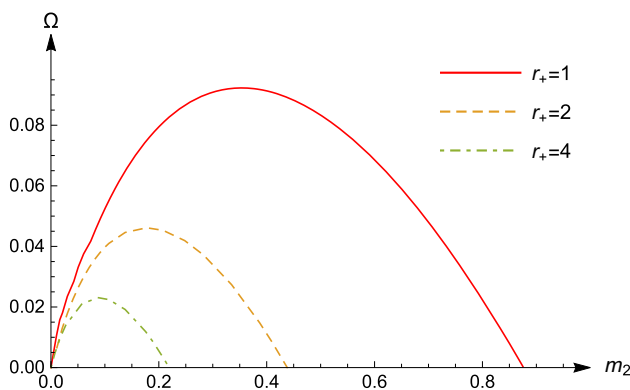

Fig. 7 Plots of unstable tensor modes with different horizon radii. The $y(x)$-axis denote Ω in $e^{\Omega t}$ (mass m_2 of massive spin-2 mode). Here we read off the thresholds of instability located at $m^{th} \approx 0.876, 0438, 0.219$ for $r_+ = 1, 2, 4$

As is shown in Fig. 6, all potentials develop negative region near the horizon, whereas their asymptotic limits are nonzero constants ($V_Z \to m_2^2$, $r \to \infty$). The former is similar to $V(r)$ in (15), while the latter is different from $V \to 0$ as $r \to \infty$. This may imply that the structure of scalarized black holes differs from that of non-Schwarzschild black hole (Schwarzschild black hole with Ricci-tensor hair). Solving Eq. (34) with boundary conditions, one finds unstable tensor modes from Fig. 7. From Fig. 7, the GL instability mass bound for $s(l = 0)$-mode is given by

$$0 < m_2 < m_{th} = \frac{0.876}{r_+}, \qquad (36)$$

where m_{th} represents the threshold of GL instability.

On the other hand, we confirm the precise value of m_{th} by solving the static Lichnerowicz-Ricci tensor equation as [7]

$$\Delta_L \psi_{\mu\nu} = \lambda \psi_{\mu\nu}, \qquad (37)$$

where the eigenvalue λ should be determined by requiring the existence of a normalizable eigenfunction $\psi_{\mu\nu}$. This amounts to seeking a negative eigenvalue λ for which the exponentially diverging solution $e^{\sqrt{-\lambda}}$ is absent when solving (37) [equivalently, (34) with $\omega = 0$ and $m_2^2 = -\lambda$] numerically by the shooting method. It determines $\lambda = -m_2^2 = -0.7677$, leading to $m_2 = m_{th} = 0.876$. We emphasize that there exists just one negative value of λ for which one can have a normalizable eigenfunction. Here, we note that $\lambda = -0.7677$ is relevant both to the edge of the zone of Schwarzschild instability and the existence of non-Schwarzschild black holes. Importantly, this process is very similar to Sect. 4 for determining α_{th} in the EMS theory. The difference is that many branches of $\alpha = \{8.019, 40.84, 99.89, \cdots\}$ for $q = 0.7$ exist in the EMS theory, while a single branch of $m_2^2 = 0.7677$ exists for the EW gravity. This may be so because their asymptotic forms of potentials are different ($V \to 0$ versus $V_Z \to m_2^2$ as $r \to \infty$). Hence, the boundary condition at infinity is an asymptotically vanishing scalar ($\varphi_\infty \to 0$) in the EMS theory, while it is a normalizable mode in the EM gravity. An actual correspondence would be met if one includes a mass term of $V(\phi) = 2\alpha\phi^2$ in (1), leading to the $s(l = 0)$-mode potential

$$V_{cp}(r) = f(r)\left[\frac{2M}{r^3} + \alpha - (\alpha + 2)\frac{Q^2}{r^4}\right], \qquad (38)$$

which has similar asymptote ($V_{cp} \to \alpha$ as $r \to \infty$) to $V_Z(r)$ in (35).

From (36), selecting $m_{th} = 1$ for $r_+ = r_c = 0.876$, one finds the bound for unstable (small) black holes

$$r_+ < r_c. \qquad (39)$$

It is worth noting that $r_+ = r_c$ corresponds to the bifurcation point which allow a new non-Schwarzschild black hole [25]. At this stage, we note that the appearance of non-Schwarzschild black hole is closely related to the threshold of instability for Schwarzschild black hole in the Einstein-Weyl gravity [6,8].

We summarize whole properties for instability happened in the EMS theory and Einstein-Weyl gravity in Table 1. It is emphasized that the role of s-mode scalars φ in the EMS theory is replaced by a s-mode Ricci tensor $\delta R_{\mu\nu}(\tilde{\varphi}_0)$ in the Einstein-Weyl gravity.

6 Scalarized RN black holes

6.1 Exponential coupling

Before we proceed, we note that the RN black hole solution is allowed for any value of α, while a scalarized RN black

Table 1 Gregory-Laflamme (GL) instability among RN black hole (RNBH) in EMS theory and and Schwarzschild black hole (SBH) in Einstein-Weyl gravity. LR denotes Licherowicz-Ricci tensor

Theory	Einstein-Maxwell-scalar theory	Einstein-Weyl gravity
Action	S_{EMS} in (1)	S_{EW} in (30)
BH without hair	RNBH with $\bar{\phi} = 0$	SBH with $\bar{R}_{\mu\nu} = 0$
Linearized equation	Scalar equation (9)	LR-equation (31)
GL instability mode	s-mode of φ	s-mode of $\delta R_{\mu\nu}$
Bifurcation points	$\alpha = 8.019, 40.84, 99.89, \cdots$ for $q = 0.7$	$m_2^2 = 0.7677$
Potential and its asymptotic form	$V(r)$ in (15) and $V_{r\to\infty} = 0$	$V_Z(r)$ in (35) and $V_{Z,r\to\infty} = m_2^2$
GL instability bound	$\alpha > \alpha_{th}(q)$ in (20)	$0 < m_2 < \frac{0.876}{r_+}$ in (36)
Small unstable BH	$r_+ < r_c = 1.714$ with $\alpha_{th} = 8.019(q = 0.7)$	$r_+ < r_c = 0.876$ with $m_{th} = 1$
BH with hair	Scalarized RN BH	Non-Schwarzschild BH

hole solution may exist only for $\alpha \geq \alpha_{th}$. The threshold of instability for a RN black hole reflects the disappearance of zero crossings in the perturbed scalar profiles. We explore a close connection between the instability of a RN black hole without scalar hair and appearance of a scalarized RN black hole. As a concrete example, we wish to find a scalarized RN black hole which is closely related to the $q = 0.7(M = 1, Q = 0.7)$ and $\alpha \geq 8.019$ case ($n = 0$ case).

For this purpose, let us introduce the metric ansatz as [9]

$$ds_{sRN}^2 = -N(r)e^{-2\delta(r)}dt^2 + \frac{dr^2}{N(r)} + r^2(d\theta^2 + \sin^2\theta d\chi^2), \tag{40}$$

where a metric function is defined by $N(r) = 1 - 2m(r)/r$ with the mass function $m(r)$. Also, we consider the $U(1)$ potential and the scalar as $A = v(r)dt$ and $\phi(r)$. Substituting these into Eqs. (2)–(4) leads to the four equations

$$-2m'(r) + e^{2\delta(r)+\alpha\phi(r)^2}r^2v'(r)^2 + [r^2 - 2rm(r)]\phi'(r)^2 = 0, \tag{41}$$

$$\delta'(r) + r\phi'(r)^2 = 0, \tag{42}$$

$$v'(r) + e^{-\delta(r)-\alpha\phi(r)^2}\frac{Q}{r^2} = 0, \tag{43}$$

$$e^{2\delta(r)+\alpha\phi(r)^2}r^2\alpha\phi(r)v'(r)^2 + r[r - 2m(r)]\phi''(r)$$
$$-\Big(m(r)[2 - 2r\delta'(r)] + r[-2 + r + 2m'(r)]\delta'(r)\Big)\phi'(r)$$
$$= 0. \tag{44}$$

Assuming the existence of a horizon located at $r = r_+$, one finds an approximate solution to equations in the near horizon

$$m(r) = \frac{r_+}{2} + m_1(r - r_+) + \cdots, \tag{45}$$

$$\delta(r) = \delta_0 + \delta_1(r - r_+) + \cdots, \tag{46}$$

$$\phi(r) = \phi_0 + \phi_1(r - r_+) + \cdots, \tag{47}$$

$$v(r) = v_1(r - r_+) + \cdots, \tag{48}$$

where the four coefficients are given by

$$m_1 = \frac{e^{-\alpha\phi_0^2}Q^2}{2r_+^2}, \quad \delta_1 = -r_+\phi_1^2,$$

$$\phi_1 = \frac{\alpha\phi_0 Q^2}{r_+(Q^2 - e^{\alpha\phi_0^2}r_+^2)}, \quad v_1 = -\frac{e^{-\delta_0-\alpha\phi_0^2}Q}{r_+^2}. \tag{49}$$

This approximate solution involves two parameters of $\phi_0 = \phi(r_+)$ and $\delta_0 = \delta(r_+)$, which will be found when matching (45)–(48) with the asymptotic solutions in the far region

$$m(r) = M - \frac{Q^2 + Q_s^2}{2r} + \cdots, \quad \phi(r) = \phi_\infty + \frac{Q_s}{r} + \cdots,$$

$$\delta(r) = \frac{Q_s^2}{2r^2} + \cdots, \quad v(r) = \Phi + \frac{Q}{r} + \cdots, \tag{50}$$

where Q_s and Φ denote the scalar charge and the electrostatic potential, in addition to the ADM mass M and the electric charge Q. For simplicity, we choose $\phi_\infty = 0$ here.

The EMS theory admits the RN black hole solution for any α. However, it becomes an unstable black hole for $\alpha > \alpha_{th}(q)$ (20), while it is stable against the scalar perturbation for $\alpha < \alpha_{th}(q)$. We note that '$\alpha = \alpha_{th}(q)$' indicates the threshold of instability. One expects that a scalarized RN black hole is allowed for $\alpha \geq \alpha_{th}(q)$ when $q \geq 0.7$. This means that the scalarized RN black holes bifurcates from the RN black hole hole at $\alpha = \alpha_{th}(q)$, but q increases beyond unity for the fixed α, implying that the scalarized RN black hole could be overcharged [9].

For the RN black hole with $\phi_0 = 0$, the outer horizon is located at $r_+ = 1.714$ and the charge-mass ratio is given by $q = 0.7$. In the Fig. 8 (left), one observes that for given $\alpha = 8.019$, the ratio of q for the $n = 0$ scalarized RN black hole increases beyond the extremal RN black hole ($q = 1$) as ϕ_0 increases. Moreover, in the Fig. 8 (right), the scalar at the horizon ϕ_0 increases as the horizon radius r_+ decreases. The scalar at the horizon is terminated at $r_+ = 1.714$, corresponding to the RN outer horizon. It is the starting point for

Fig. 8 (left) The charge-mass ratios q of the $n = 0$ scalarized RN black hole as functions of ϕ_0 with the fixed $\alpha = 8.019$ for exponential and quadratic couplings. The horizontal line represents the maximum ratio $q = 1$ for the RN black hole. (right) The scalars at the horizon ϕ_0 as functions of the horizon radius r_+ for the $n = 0$ scalarized black hole
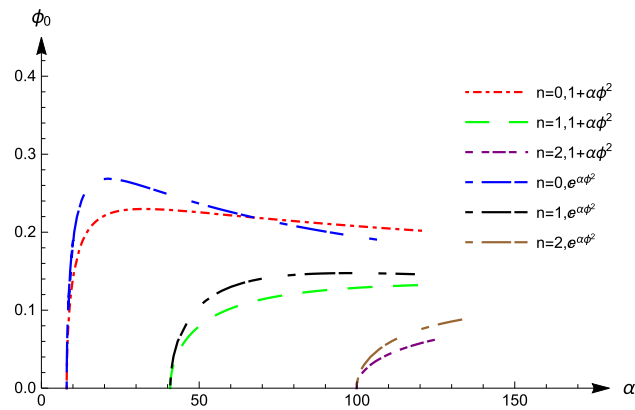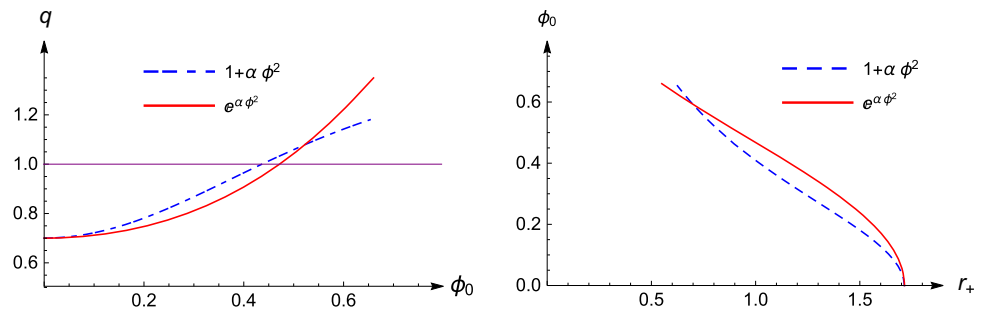

Fig. 9 The scalar field $\phi_0 = \phi(r_+)$ at the horizon as a function of mass-like parameter α for exponential and quadratic couplings . All the nontrivial branches with $n = 0, 1, 2$ start from bifurcation points at $\alpha_n = \{8.019, 40.84, 99.89\}$ on the trivial branch (RN black holes on α-axis). They span the whole region without upper bound

a scalarized RN black hole, while from (21) it corresponds to the ending point for unstable RN black hole.

It is known that the scalarization bands exist for the ESGB theory [2]. A discrete set for η/M^2 obtained from static scalar perturbation corresponds to the right-end values of scalarization bands for a scalarized Schwarzschild black hole, while the left-end values are provided by the regularity constraint at the horizon ($r_+^4 \geq 6\eta^2\phi_0^2$). However, as is shown in Fig. 9, there are no scalarization bands in the EMS theory because we do not need to impose the regularity condition at the horizon. As a result, there is no upper bound on α as $n = 0(\alpha \geq 8.019)$, $1(\alpha \geq 40.84)$, and $2(\alpha \geq 99.89)$.

Consequently, we obtain the scalarized RN black hole solution depicted in Fig. 10. The metric function $N(r)$ has a different horizon at $\ln r = \ln r_+ = 0.067$ in compared to the RN horizon at $\ln r = \ln r_+ = 0.539$ and it approaches the RN metric function $f(r)$ as $\ln r$ increases. Also, the scalar hair $\phi(r)$ starts with $\phi_0 = 0.44$ at the horizon and it decreases as $\ln r$ increases, in compared to $\phi(r) = 0$ for the RN black hole.

6.2 Quadratic coupling

Considering the quadratic coupling of $\alpha\phi^2$, we have to choose $\bar{\phi} = $ const to obtain the RN black hole with dif-

ferent charge $\tilde{Q}^2 = \alpha\bar{\phi}^2 Q^2$. In order to make the analysis simple, we may choose an equivalent coupling of $1 + \alpha\phi^2$ with $\bar{\phi} = 0$ to give the RN black hole. In this case, the bifurcation points of the RN solution are the same as those of exponential coupling because the static scalar equation takes the same form as in (22). Furthermore, instabilities of RN solution are exactly the same for both couplings. To obtain scalarized RN black holes, we solve Eqs. (41)–(44) by replacing $e^{\alpha\phi^2}$ with $1 + \alpha\phi^2$. From Figs. 8, 9, 10, we observe that the quadratic coupling shows the similar properties to the exponential coupling.

As was mention in [26], however, the only difference between two coupling in the ESGB theory is that the $n = 0$ fundamental branch of scalarized black holes is stable for the exponential coupling, while the $n = 0$ fundamental branch is unstable for the quadratic coupling. Therefore, we expect that the similar thing will happen since the $n = 0$ scalarized RN black hole turned out to be unstable in the EMS theory with exponential coupling [27].

7 Discussions

First of all, we mention that scalarized RN black holes were found in the EMS theory. It is emphasized that the appearance of these black holes with scalar hair is closely related to the instability of the RN black hole without scalar hair in the EMS theory. Concerning the appearance scalarized RN black holes [9], it is very important to obtain the precise threshold α_{th} of instability for the RN black hole in the EMS theory. In this work, we have obtained the GL instability bound (20) for the RN black hole in the EMS theory by considering $s(l = 0)$-mode scalar perturbation.

Roughly speaking, a shape of scalar potential $V(r)$ in (15) determines the instability of RN black hole. The sufficient condition of $\int_{r_+}^{\infty} dr[V(r)/f(r)] < 0$ for instability [18,19] gives rises to an analytic bound (16), while the sufficient condition for stability is given by the other bound (17). Explicitly, for $q = 0.418$, the sufficient condition for instability takes the form of $\alpha > 30.74$, whereas the sufficient condition for the stability is given by $0 < \alpha \leq 19.83$. In the case of $\int_{r_+}^{\infty} dr[V(r)/f(r)] > 0$ with negative potential near
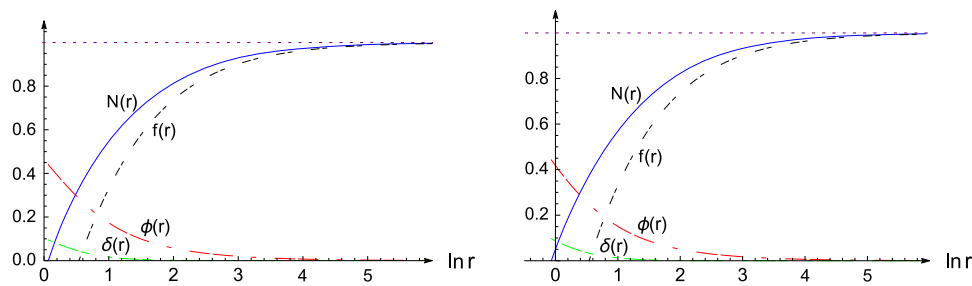
Fig. 10 The $n = 0$ scalarized RN solutions. (left) Exponential coupling. Two metric functions $f(r)$ for RN and $N(r)$ for scalarized RN are given by functions of r for $\alpha = 8.019$. We observe that the logarithmic values of horizon radius of scalarized RN and RN black holes are located at 0.067 and 0.539, respectively. The scalar hair $\phi(r)$ starts with $\phi_0 = 0.44$ at the horizon and it decreases as $\ln r$ increases. (right) Quadratic coupling. The logarithmic values of horizon radius of scalarized RN and RN black holes are located at -0.062 and 0.539, respectively

the horizon, however, it is not easy to make a clear decision on the stability of the black hole. Here it is still stable for $19.83 < \alpha \leq 29.47$ with $q = 0.418$ even providing negative region near the horizon shown in Fig. 1. In this case, the S-deformation method might provide a complementary result to support the stability of such black holes by finding the deformed potential [21,22].

In general, the GL instability bound is not given by an analytic form. As was shown in Fig. 3 depending on q, it was determined by solving the linearized Eq. (9) numerically. In the case of $q = 0.418$, the GL instability bound is $\alpha > 29.47$ which is surely less than the sufficient condition for instability ($\alpha > 30.74$). Importantly, this picture shows that the GL instability appeared in a simpler EMS theory than the ESGB theory and Einstein-Weyl gravity. For $q = 0.7$, we have obtained the GL instability bound of $\alpha > \alpha_{\text{th}} = 8.019$. We have derived the precise value of threshold $\alpha_{\text{th}} = 8.019$ again by solving the static linearized equation numerically. Furthermore, we have obtained the $n = 0(\alpha \geq 8.019)$ scalarized RN black hole by solving Eqs. (41)–(44) numerically for exponential and quadratic couplings.

Consequently, we have explored a clear connection between GL instability of RN black hole and scalarization of RN black hole.

Data Availability Statement This manuscript has no associated data or the data will not be deposited. [Authors' comment: This is a theoretical study and experimental data has not been listed.]

References

1. D.D. Doneva, S.S. Yazadjiev, Phys. Rev. Lett. **120**(13), 131103 (2018). https://doi.org/10.1103/PhysRevLett.120.131103. arXiv:1711.01187 [gr-qc]
2. H.O. Silva, J. Sakstein, L. Gualtieri, T.P. Sotiriou, E. Berti, Phys. Rev. Lett. **120**(13), 131104 (2018). https://doi.org/10.1103/PhysRevLett.120.131104. arXiv:1711.02080 [gr-qc]
3. R. Gregory, R. Laflamme, Phys. Rev. Lett. **70**, 2837 (1993). https://doi.org/10.1103/PhysRevLett.70.2837. arXiv:hep-th/9301052
4. Y.S. Myung, D.C. Zou, Phys. Rev. D **98**(2), 024030 (2018). https://doi.org/10.1103/PhysRevD.98.024030. arXiv:1805.05023 [gr-qc]
5. B. Whitt, Phys. Rev. D **32**, 379 (1985). https://doi.org/10.1103/PhysRevD.32.379
6. Y.S. Myung, Phys. Rev. D **88**(2), 024039 (2013). https://doi.org/10.1103/PhysRevD.88.024039. arXiv:1306.3725 [gr-qc]
7. H. L, A. Perkins, C. N. Pope, K. S. Stelle, Phys. Rev. D **96**(4), 046006 (2017). https://doi.org/10.1103/PhysRevD.96.046006. arXiv:1704.05493 [hep-th]
8. K.S. Stelle, Int. J. Mod. Phys. A **32**(09), 1741012 (2017). https://doi.org/10.1142/S0217751X17410123
9. C.A.R. Herdeiro, E. Radu, N. Sanchis-Gual, J.A. Font, Phys. Rev. Lett. **121**(10), 101102 (2018). https://doi.org/10.1103/PhysRevLett.121.101102. arXiv:1806.05190 [gr-qc]
10. I.Z. Stefanov, S.S. Yazadjiev, M.D. Todorov, Mod. Phys. Lett. A **23**, 2915 (2008). https://doi.org/10.1142/S0217732308028351. arXiv:0708.4141 [gr-qc]
11. D.D. Doneva, S.S. Yazadjiev, K.D. Kokkotas, I.Z. Stefanov, Phys. Rev. D **82**, 064030 (2010). https://doi.org/10.1103/PhysRevD.82.064030. arXiv:1007.1767 [gr-qc]
12. F.J. Zerilli, Phys. Rev. D **9**, 860 (1974). https://doi.org/10.1103/PhysRevD.9.860
13. V. Moncrief, Phys. Rev. D **9**, 2707 (1974). https://doi.org/10.1103/PhysRevD.9.2707
14. V. Moncrief, Phys. Rev. D **10**, 1057 (1974). https://doi.org/10.1103/PhysRevD.10.1057
15. V. Moncrief, Phys. Rev. D **12**, 1526 (1975). https://doi.org/10.1103/PhysRevD.12.1526
16. E.W. Hirschmann, L. Lehner, S.L. Liebling, C. Palenzuela, Phys. Rev. D **97**(6), 064032 (2018). https://doi.org/10.1103/PhysRevD.97.064032. arXiv:1706.09875 [gr-qc]
17. C. Pacilio, Phys. Rev. D **98**(6), 064055 (2018). https://doi.org/10.1103/PhysRevD.98.064055. arXiv:1806.10238 [gr-qc]
18. W.F. Buell, B.A. Shadwick, Am. J. Phys. **63**, 256 (1995)
19. G. Dotti, R.J. Gleiser, Class. Quant. Grav. **22**, L1 (2005). https://doi.org/10.1088/0264-9381/22/1/L01. arXiv:gr-qc/0409005

20. H. Kodama, A. Ishibashi, Prog. Theor. Phys. **111**, 29 (2004). https://doi.org/10.1143/PTP.111.29. arXiv:hep-th/0308128

21. M. Kimura, Class. Quant. Grav. **34**(23), 235007 (2017). https://doi.org/10.1088/1361-6382/aa903f. arXiv:1706.01447 [gr-qc]

22. M. Kimura, T. Tanaka, Class. Quant. Grav. **35**(19), 195008 (2018). https://doi.org/10.1088/1361-6382/aadc13. arXiv:1805.08625 [gr-qc]

23. E. Babichev, A. Fabbri, Class. Quant. Grav. **30**, 152001 (2013). https://doi.org/10.1088/0264-9381/30/15/152001. arXiv:1304.5992 [gr-qc]

24. R. Brito, V. Cardoso, P. Pani, Phys. Rev. D **88**(2), 023514 (2013). https://doi.org/10.1103/PhysRevD.88.023514. arXiv:1304.6725 [gr-qc]

25. H. Lu, A. Perkins, C.N. Pope, K.S. Stelle, Phys. Rev. Lett. **114**(17), 171601 (2015). https://doi.org/10.1103/PhysRevLett.114.171601. arXiv:1502.01028 [hep-th]

26. J.L. Blzquez-Salcedo, D.D. Doneva, J. Kunz, S.S. Yazadjiev, Phys. Rev. D **98**(8), 084011 (2018). https://doi.org/10.1103/PhysRevD.98.084011. arXiv:1805.05755 [gr-qc]

27. Y.S. Myung, D.C. Zou, Phys. Lett. B **790**, 400 (2019). https://doi.org/10.1016/j.physletb.2019.01.046. arXiv:1812.03604 [gr-qc]